Innovative Double-Wedging Mechanism for Die-Cutting Presses: CAD/CAE-based Kinematic and Force Analysis

Ivan Rehei
Dr. Sc, Professor
Institute of Printing and Media Technologies
Lviv Polytechnic National University
Ukraine

Oleh Knysh
Dr. Sc, Professor
Institute of Printing and Media Technologies
Lviv Polytechnic National University
Ukraine

Vitalii Vlakh
Ph.D.
Independent Researcher
Canada

Andrii Ternovyi
Graduate Student
Institute of Printing and Media Technologies
Lviv Polytechnic National University
Ukraine

This paper presents the design and analysis of a novel double-wedging drive mechanism for the pressure plate of a die-cutting press, proposed as an alternative to traditional crankshaft systems. The mechanism improves motion transmission, increases contact uniformity with the cardboard sheet, and reduces inertial loads during embossing, creasing, and cutting. A kinematic scheme is developed, and analytical expressions for displacement and torque are derived. A custom Python tool automates parameter calculation, model generation, and integration with SolidWorks for simulation and optimization. 3D models and motion studies validate the analytical model. A force analysis confirms the mechanism's structural feasibility. The proposed system ensures more stable, efficient pressure plate motion, thereby enhancing die-cutting press performance. The integration of Python automation with CAD/CAE tools improves the engineering workflow and supports future industrial implementation.

Keywords: *die-cutting press, forces, wedging mechanism, kinematics, automation, SolidWorks, Python, simulation*

1. INTRODUCTION

The packaging industry is one of the most dynamic sectors of modern manufacturing, continuously evolving in response to changes in consumer behaviour, tech–nological innovations, and global environmental chal–lenges. A substantial portion of today's packaging is made of cardboard, a material valued for its techno–logical efficiency, recyclability, and eco-friendliness. Due to its rigidity, lightweight structure, and precise formability, cardboard packaging is widely used in the food, pharmaceutical, cosmetic, household, and logistics sectors [1].

1.1 Packaging Industry Context and Related Research

The environmental performance of cardboard packaging involves selecting raw materials and designing struc–tures, considering recycling behaviour [2]. In the con–text of the global transition toward sustainable manu–facturing, the adoption of "green" approaches in packaging production is becoming increasingly promi–nent. Key areas of development include waste reduc–tion, the use of environmentally friendly lubricants, energy-efficient material processing technologies, and the implementation of product life cycle principles [3].

A critical step in making cardboard packaging is die-cutting. This process shapes a blank piece of cardboard into the required form. After die-cutting, the cardboard is folded and assembled into the final product. The precision and stability of this process directly impact the final product's quality. Today, die-cutting mechanisms face increased demands for pressure uniformity, positional accuracy, and compatibility with automated lines [4]. In recent years, there has also been a surge in innovative technologies applied to cardboard packaging, along with a substantial shift toward sustainable prac–tices. These include minimizing waste and optimizing design to enhance recyclability [5]. Die-cutting equip–ment continues to evolve from traditional presses to digitally controlled servo systems [6]. There is growing interest in technologies that enable even pressure dist–ribution, accurate pressure control, reduced tool wear, and improved energy efficiency. Advances in cardboard packaging have driven active research into improving die-cutting press mechanisms to enhance accuracy, reliability, and productivity. Packaging increasingly serves both functional and marketing purposes, further raising expectations for precision in material treatment.

Die-cutting remains a critical operation in cardboard packaging, directly influencing blank dimensions, fol–dability, and overall product quality. Over the last decade, researchers have concentrated on enhancing press drive mechanisms, reducing inertial forces, imp–roving dynamic stability, and introducing alternative drive concepts.

The most common drive system for die-cutting pres–ses is a wedging mechanism that drives the pressure plate. Its kinematics have been studied extensively. In work [7], the authors used vector analysis and simula–tion in MATLAB and ADAMS to study the system. They showed that substantial inertial forces arise at high speeds (6000 cycles/hour), limiting the mechanism's durability and precision.

A significant problem with traditional mechanisms is the high peak accelerations in components (up to 40

Received: August 2025, Accepted: December 2025
Correspondence to: Vitalii Vlakh, Ph.D.
Independent Researcher
Canada
E-mail: vlakh.v.v@gmail.com
doi: 10.5937/fme2601070R

rad/s²), which result in impact loads and rapid wear. SolidWorks simulations confirm high stresses and de–formation in key links. The authors proposed a con–jugate cam mechanism as an alternative to conventional crankshaft systems.

In article [8], the motion of the press's moving platform relative to the crankshaft angle was modelled. Using a 3D CAD model, they established clear phase relationships between displacement, velocity, and acce–leration and identified critical load zones. This work forms the basis for further motion optimization and cyclic kinematic refinement. Recent studies have app–lied materials engineering methods (e.g., QFD, axio–matic design) and multi-objective optimization. In work [9], a lightweight rocker arm with optimized geometry was proposed, reducing mass by 27% while preserving stiffness. That cut deformation from 0.096 mm to 0.0098 mm, boosting precision at 7500 cycles/hour. Using NSGA-II optimization, they balanced weight and stiffness, and dynamic modelling confirmed stable press operation.

In [10], the authors presented a concept for moder–nizing the pressure plate drive by introducing a pneu–matic mechanism. The study substantiates the use of four synchronized pneumatic cylinders to ensure planar-parallel plate movement with minimal energy consum–ption. Additionally, a design incorporating perforated channels at the base of the plate was proposed to create an air-cushion effect during die-cutting, thereby pro–longing the lifespan of cutting tools. The authors emphasize that this design represents an energy-efficient alternative to conventional mechanical drives, reduces contact loads, and is suitable for industrial imple–mentation.

Over the past several years, the authors of this article have conducted a series of studies to improve the drive mechanisms of pressure plates in die-cutting equipment. The results of these investigations have laid the scientific foundation for further enhancing die-cutting presses, particularly regarding the execution of embossing operations on cardboard. All projects share the common objective of reducing technological loads, improving the precision of plate motion, and enhancing the operational stability of the equipment, especially when processing complex, multilayer cardboard materials.

Study [11] focuses on examining the motion characteristics of the pressure plate driven by wedging mechanisms. Based on the results of the geometric synthesis of the mechanism, a mathematical model of the oscillatory motion of the plate during the working and idle strokes was developed. It was determined that in the initial crank position, the angular displacement amplitude of the plate reaches ±2.125°, whereas at the phase angle $\varphi = 135°$, the plate is in a horizontal position. The relative displacements of the left and right sides of the plate were also calculated, $Sc1i = 0.095$ and $Sc2i = 0.327$, respectively, confirming the presence of oscillatory motion in conventional drive configurations.

Study [12] experimentally determined the torque values acting on the drive shaft of the pressure plate equipped with eccentric mechanisms. For cardboard thicknesses ranging from 0.3 to 0.7 mm and a speed of up to 120 cycles per minute, peak torque values reached 21.5 N·m, with 85-90% of the load attributed to the technological component. Accurate relationships were obtained between torque and cardboard thickness, with a model error not exceeding 9%.

In [13], a screw-nut transmission system was pro–posed for the pressure plate drive. A physical prototype of the drive was constructed, incorporating a non-contact electronic strain gauge. It was established that the torque on the shaft was 15-20% lower for the same cardboard thickness than in the eccentric mechanism. The study also confirmed stable and flat-parallel motion of the pressure plate throughout the entire operating cycle.

Experiment [14] examined a method for cutting corrugated cardboard using a rotating cutting disc in combination with stationary counter-knives. The study demonstrated that with a tool overlap of 2-3 mm and cardboard thickness up to 7.2 mm, load torque decreased by 25%, while fluting orientation influenced load torque by 22%. These findings highlight the po–tential for applying disc-cutting technologies in auto–matic systems for manufacturing large-format corru–gated packaging.

In [15], an analytical load model was proposed that incorporates inertial, gravitational, and technological components. Torque-angle diagrams were constructed for various cutting conditions. The model was validated against data from previous experiments and demon–strated an accuracy within 10% across all examined scenarios.

Publication [16] was the first to propose a two-section pressure plate design, where each section inc–ludes eccentrics with a phase shift. This configuration allows the cardboard to gradually come into contact with the die, thereby reducing peak forces in the drive. Displacement values for the sections were calculated based on material thickness, resulting in smoother plate movement during the processing of multilayer materials.

Building on this concept, a subsequent study [17] introduced a pressure plate design with wedging mechanisms and sectional engagement. It demonstrated that phase-shifting the eccentrics enables optimal load distribution between the sections, reduces the overall dimensions of the equipment, and relaxes structural strength requirements for the machine frame.

These technical solutions lay the groundwork for further development of operations where controlled pre–ssure and precise displacement are critical, particularly in embossing processes. Embossing cardboard involves creating raised or recessed features on the surface of packaging material using a pair of tools: a die and a punch. This type of processing is employed not only for decorative enhancement of packaging but also for functional marking, such as Braille text.

The shape of the tools determines the quality of embossing, the properties of the cardboard, and the precision with which process parameters, specifically pressure and dwell time, are maintained. The visual and tactile clarity of the embossed image depends on material characteristics, tool geometry, temperature, pressure, and contact duration. Contemporary research shows that results can vary significantly, even with

identical tool shapes, depending on the material's structure and process conditions. One of the fundamental physical principles of embossing is the cardboard's ability to undergo plastic deformation under compression and its partial recovery upon unloading [18].

The application of additional energy, such as ultrasonic vibrations, has emerged as a promising approach to enhance the precision and depth of embossing. Under ultrasonic excitation, the fibrous structure of cardboard temporarily alters its mechanical properties, allowing for clearer relief formation with reduced force and lower energy consumption [19].

Experimental comparisons between conventional and ultrasonic embossing confirm the advantages of these new approaches, particularly in terms of embossing depth, reduced elastic recovery of the material, and improved consistency of results. Such technologies expand the potential applications of embossing in packaging and open new opportunities for processing complex and multilayer materials [20].

1.2 Recent Research and Motivation

A review of current research on embossing reveals that most studies focus on the mechanical and physical properties of cardboard, the geometry of embossing tools, and the application of new energy-assisted technologies (e.g., ultrasound) to enhance the accuracy of relief formation. However, nearly all of these investigations are based on conventional drive schemes for the pressure plate, which inherently suffer from limitations such as oscillatory plate motion and insufficient contact time with the material.

In addition, many recent studies evaluate cutting/embossing quality primarily through material behaviour, tool geometry, or energy-assisted methods, while treating the pressure-plate drive as a fixed, conventional subsystem. As a result, key practical limitations remain insufficiently addressed: the oscillatory motion of the pressure plate, which reduces alignment repeatability and increases setup sensitivity; limited contact (dwell) time, which constrains creasing/embossing quality; and the lack of scalable, parameterized design procedures that can be quickly adapted to different press formats while keeping kinematics and torque within acceptable limits. These gaps motivate the development of an alternative drive concept with extended contact duration, improved motion regularity, and a workflow that couples analytical synthesis with CAD/CAE validation.

Our research addresses these issues by improving the wedging mechanisms of the pressure plate drive. The primary goal is to ensure smooth, controlled movement of the pressure plate and to extend its contact time with the material during the embossing and creasing phases. This is particularly critical for achieving high-quality relief formation and well-defined creasing lines, especially in producing cardboard layouts using traditional die-cutting presses that perform "cold" embossing alongside cutting and creasing.

Extended contact between the punch and the die with the cardboard significantly enhances the quality of the embossed elements and densified creasing lines. A related issue is the need for strictly vertical movement of the pressure plate. A promising direction involves the development of a modular pressure plate drive. This approach enables the creation of a series of die-cutting machines with different formats based on standardized and unified modules.

This direction has been consistently developed and validated in our recent publications [21–23], which are briefly summarized below. In publication [21], a design incorporating an additional crank in the driven link of the mechanism is proposed. This modification enables the regulation of angular motion parameters. It extends the contact phase between the die-cutting form and the cardboard by 1.4 times compared to the baseline mechanism. Such a design enables the pressure plate to adapt to combined technological processes, including die-cutting, creasing, and embossing.

Study [22] presents a comparative analysis of the conventional wedging mechanism and the improved configuration with an auxiliary crank, performed through SolidWorks modelling. The study demonstrates that the contact time between the forming tools and cardboard increases by 12% in the proposed design. At the same time, the maximum acceleration at the end of the working stroke decreases by a factor of 3.43. These improvements significantly enhance the embossing conditions.

In [23], a geometric synthesis and analytical calculation of a combined mechanism featuring dual wedging contours, a pair of auxiliary cranks, and gear transmissions were conducted. Virtual modelling in SolidWorks validated the results, confirming high accuracy. It was shown that contact between the tool and single-layer cardboard is maintained for 56° of crank rotation, corresponding to 16% of the total cycle time, substantially improving the embossing performance for cardboard blanks.

The **scientific contribution** of this work is the development of a novel double-wedging pressure-plate drive concept together with a consistent analytical framework for its kinematic and torque evaluation. The engineering contribution is a practical, parameterized design and verification workflow: the derived equations are implemented in a Python tool that automatically computes key geometry, updates the CAD model, and runs SolidWorks Motion studies to validate displacements, velocities, accelerations, and resisting torques. This enables faster mechanism tuning for different press formats and supports more stable pressure-plate motion and extended contact duration required for high-quality creasing and embossing.

2. METHODOLOGY

General trends in contemporary mechanism kinematics research focus on enhancing the capabilities of classical structures, including compliant systems, tensegrity mechanisms, and the synthesis of high-complexity spatial linkages. As noted in [24], the development of algebraic methods, particularly polynomial continu–ation, enables the solution of systems with millions of potential outcomes, opening new possibilities for the design of complex actuators. These approaches lay the groundwork for creating unconventional actuator configurations, such as the double-wedging actuator proposed in this study.

A comparable approach of integrating compliant structures with rigid motion transmission was explored for continuum manipulators, demonstrating how tailored linkage architectures can achieve uniform, controllable motion with high dexterity and extensibility [25]. Similar to wire-actuated surgical manipulators, the pro–posed mechanism benefits from analysing transition effects in load-bearing links, where tension-based dis–continuities may lead to motion inaccuracies if not accounted for properly [26].

Recent advances in compliant mechanism design, such as meso-scale grippers with passive adaptation, emphasize the importance of consistent contact and adaptive motion, which parallels the goals of our proposed pressure plate mechanism [27]. A novel double-wedging drive mechanism has been developed to implement the above motion control objectives. This configuration ensures controlled linear movement of the pressure plate, improved symmetry in load distribution, and increased contact duration between the die tools and the cardboard. The mechanism consists of mirrored left and right transmission circuits that interact to maintain stability and precision.

2.1 Mechanism Description

The kinematic diagram of the double-wedging drive mechanism for the pressure plate of a die-cutting press is shown in Fig. 1. The mechanism consists of the upper stationary plate (1) with the flat die (2), the moving pressure plate (3), and the wedging and drive mecha–nisms for the left and right contours.

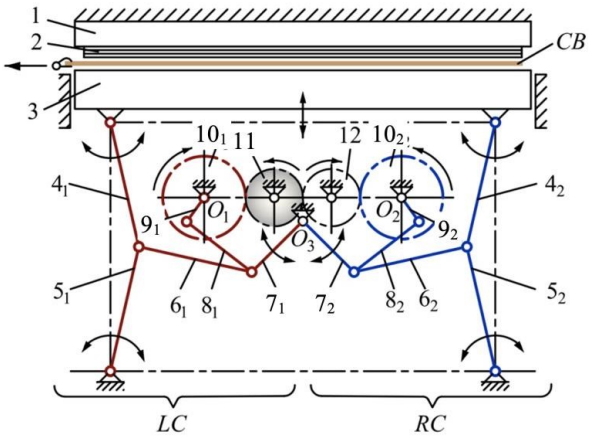

Figure 1. Kinematic scheme of the double-wedging drive mechanism of the pressure plate in a die-cutting press

The drive of the pressure plate on the left contour (LC) consists of an upper wedging lever(4_1) and a lower wedging lever (5_1) forming the vertical wedging mec–hanism, and the left (6_1) and right (7_1) levers forming the horizontal wedging mechanism. The drive of the pressure plate on the right contour (RC) includes the upper (4_2) and lower (5_2) levers of the vertical wedging mechanism and the right (6_2) and left (7_2) levers of the horizontal wedging mechanism.

The actuation of the wedging mechanisms in the left contour is ensured by a hinged connection between the left connecting rod (8_1) and the left crank (9_1). Similarly, the right contour's wedging mechanisms are actuated via a hinged connection between the right connecting rod (8_2) and the right crank (9_2).

The left crank (9_1) is mounted on the left shaft O_1 together with the left gear wheel (10_1), while the right crank (9_2) is mounted on the right shaft O_2 along with the right gear wheel (10_2). The driving gear is a gear wheel (11), which meshes on the left with gear (10_1) and on the right with an idler gear (12) that, in turn, engages with the right gear wheel (10_2). The die-cutting press operates as follows. In the initial position, the pressure plate (3) and the cardboard blank (CB) are located at their bottom-most position. When the driving gear wheel (11) rotates counterclockwise, the left gear wheel (10_1) of the left contour (LC) rotates clockwise, driving the left crank (9_1) and the left connecting rod (8_1). Through a hinged connection, this motion causes the horizontal and vertical wedging mechanisms of the left contour to actuate, aligning the levers (6_1, 7_1) and (4_1, 5_1), respectively. Simultaneously, the motion from the driving gear wheel (11) is transmitted through the idler gear (12) to the driven right gear wheel (10_2) of the right contour (RC), which rotates counterclockwise. Gear (10_2) actuates the right crank (9_2) and connecting rod (8_2), which, through their hinged connection, initiate the actuation of the horizontal and vertical wedging mechanisms on the right side, aligning the levers (6_2, 7_2) and (4_2, 5_2).

Simultaneously aligning the wedging mechanism levers on both the left (LC) and right (RC) contours lifts the pressure plate (3) and performs die-cutting of the cardboard blank (CB) at its topmost position.

Further counterclockwise rotation of the driving gear wheel (11) reduces the angles between the wedging mechanism links, which results in lowering the pressure plate (3). This lowering motion allows for the removal of the die-cut cardboard blank (CB) and the feeding of a new blank into the die-cutting zone.

2.2 Geometric Synthesis of the Mechanism

The pressure plate is actuated by two identical com–bined mechanisms on the left (LC) and right (RC) contours. Therefore, the geometric synthesis and the analysis of kinematic and force relationships are con–ducted for one (left) contour only (Fig. 2).

For the analytical synthesis of the sub-contours in the combined double-wedging mechanism of the left drive contour, the following relative parameters are defined:

S = 1.0 - maximum displacement of the pressure plate (Fig. 2 b);

W_0 = 5.0 - horizontal distance between the supports of the double-wedging mechanism on the left contour;

H_0 = 3.4 - vertical distance between the supports of the double-wedging mechanism on the left contour.

These parameters serve as the starting values for the geometric synthesis of the mechanism. The dimensions are optimized for maximum pressure plate displacement (based on real machine specifications), ensuring effi–cient operation of the mechanism.

Angular parameter notation:

ζ_0 = 5° - limiting angle for the horizontal and vertical wedging contours to prevent mechanism jamming.

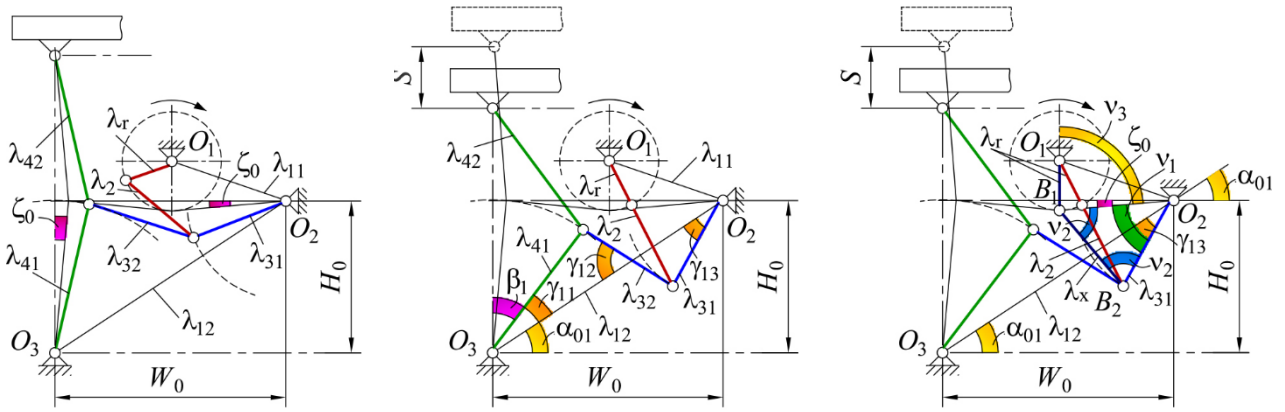

Figure 2. Kinematic schemes of the double-wedging drive mechanism of the pressure plate (left contour) in a die-cutting press for geometric synthesis: (a) links of the horizontal and vertical wedging mechanisms; (b) positions of the wedging mechanism levers relative to the inter-base axis; (c) crank and connecting rod.

For the geometric synthesis of the double-wedging mechanism, the following relative parameters of the links are introduced (Fig. 2a):

λ_{11} - base distance between axes O_1 and O_2; 314

λ_{12} - base distance between axes O_2 and O_3;

λ_r - crank radius;

λ_2 - length of the connecting rod;

λ_{31}, λ_{32} - the length of the lever and connecting rod of the horizontal wedging mechanism;

λ_{41}, λ_{42} - lengths of the lower and upper levers of the vertical wedging mechanism.

The relative lengths of the right and left levers of the horizontal wedging mechanism and the lower and upper levers of the vertical wedging mechanism are given by:

$$\lambda_{41} = \lambda_{42} = \frac{H_0}{\cos\zeta_0} \tag{1}$$

$$\lambda_{31} = \lambda_{32} = \frac{0.5\left[W_0 - \left(H_0 \cdot tg\zeta_0\right)\right]}{\cos\zeta_0} \tag{2}$$

The relative base distance between axes O_2 and O_3:

$$\lambda_{12} = \sqrt{W_0^2 + H_0^2} \tag{3}$$

The angle between base axis λ_{12} and the horizontal:

$$\alpha_{01} = arctg\frac{H_0}{W_0} \tag{4}$$

The angle between the lower lever λ_{41} of the vertical wedging mechanism and the vertical in the lower position of the pressure plate:

$$\beta_1 = \arccos\frac{H_0 - 0.5}{\lambda_{41}} \tag{5}$$

Angle between the lower lever λ_{41} and the base axis λ_{12}:]

$$\gamma_{11} = \frac{\pi}{2} - \left(\alpha_{01} + \beta_1\right) \tag{6}$$

To determine the angle between the right lever λ_{31} and the base axis λ_{12}, we use the system:

$$\begin{cases} \lambda_{41}\cos\gamma_{11} + \lambda_{32}\cos\gamma_{12} + \lambda_{31}\cos\gamma_{13} = \lambda_{12} \\ \lambda_{41}\sin\gamma_{11} + \lambda_{31}\sin\gamma_{13} = \lambda_{32}\sin\gamma_{12} \end{cases} \tag{7}$$

Solution of system (7):

$$\lambda_{13} = arc\sin\left(\frac{L\cdot N \pm 0.5\sqrt{D}}{K^2 + L^2}\right) \tag{8}$$

where:

$$L = -\lambda_{41}\cdot\sin\gamma_{11} \tag{8.1}$$

$$K = \lambda_{12} - \lambda_{41}\cos\gamma_{11} \tag{8.2}$$

$$N = \frac{K^2 + \lambda_{31}^2 + L^2 - \lambda_{32}^2}{2\lambda_{31}} \tag{8.3}$$

$$D = \left(2L\cdot N\right)^2 - 4\left(K^2 + +L^2\right)\left(N^2 - K^2\right) \tag{8.4}$$

For crank radius λ_r and connecting rod λ_2 (Fig. 2 c), assuming the pressure plate is in its bottom position:

$$\nu_1 = \gamma_{13} + \alpha_{01} - \zeta_0 \tag{9}$$

$$\nu_2 = \frac{\pi - \nu_1}{2} \tag{10}$$

$$\nu_3 = \arcsin\frac{W_0 - H_0 tg\zeta_0}{2\cdot\lambda_{31}} \tag{11}$$

Triangle $O_1B_1B_2$:

$$\lambda_x = 2\lambda_{31}\cdot\sin\frac{\nu_1}{2} \tag{12}$$

Summing $\lambda_2 = 2\lambda_r$:

$$\lambda_r = \frac{\lambda_x\left(\sqrt{\cos^2\left(\nu_2 + \nu_3\right) + 8} - \cos\left(\nu_2 + \nu_3\right)\right)}{8} \tag{13}$$

2.3 Kinematic Analysis

The kinematic analysis of the double-crank wedging mechanism on the left contour involves studying the relative displacement, velocity, and acceleration of the pressure plate. Thesynthesized input parameters are the relative geometric values obtained in Table 1.

The analysis is performed with respect to the changing crank angle φ, which defines the angular position of the crank λr relative to the base axis λ11.

Table 2 lists the analytical expressions for calculating the relative motion characteristics (Fig. 3) of the pressure plate.

The velocity of the pressure plate is defined as the derivative of its displacement, $V_i = dS/d\varphi$, and the acceleration is defined as the derivative of the velocity $wi = dV/d\varphi$.

Table 1. Relative geometric parameters of the links

No.	Parameter	Value
1	λ_{11}	2.47
2	λ_{12}	6.046
3	λ_{31}, λ_{32}	2.36
4	λ_{41}, λ_{42}	3.413
5	λ_r	0.963
6	λ_2	1.926

Table 2. Analytical Kinematic Parameters

No.	Parameter Description	Notation	Analytical Expression	Eq.
1	Initial crank angle φ_0	φ_0	$\varphi_0 = \arccos\frac{(\lambda_r+\lambda_2)^2+\lambda_{11}^2-\lambda_{31}^2}{2(\lambda_r+\lambda_2)\cdot\lambda_{11}}$	(14)
2	Auxiliary angle	$\varphi_0+\varphi_{01}$	$\varphi_0+\varphi_{01} = \arccos\frac{\lambda_r^2+\lambda_{11}^2-\lambda_{31}^2}{2\lambda_r\cdot\lambda_{11}}$	(15)
3	Max crank angle	φ_{max}	$\varphi_{\max} = \pi+\varphi_0+\varphi_1$	(16)
4	Angle λ_{11} to λ_{31} (bottom)	γ_{01}	$\gamma_{01} = \arccos\frac{\lambda_{11}^2+\lambda_{31}^2-(\lambda_r+\lambda_2)^2}{2\lambda_{11}\cdot\lambda_{31}}$	(17)
5	Angle λ_{11} to λ_{31} (top)	γ_{02}	$\gamma_{02} = \arccos\frac{\lambda_{31}^2+\lambda_{11}^2-\lambda_r^2}{2\lambda_{31}\cdot\lambda_{11}}$	(18)
6	Axis between O_2 and joint A	Δ	$\Delta = \sqrt{\lambda_r^2+\lambda_{11}^2-2\lambda_r\cdot\lambda_{11}\cdot\cos\varphi}$	(19)
7	Angle Δ to λ_{11}	γ_{04}	$\gamma_{04} = \arccos\frac{\Delta^2+\lambda_{11}^2-\lambda_r^2}{2\Delta\cdot\lambda_{11}}$	(20)
8	Angle Δ to λ_2	γ_{05}	$\gamma_{05} = \arccos\frac{\Delta^2+\lambda_2^2-\lambda_{31}^2}{2\Delta\cdot\lambda_2}$	(21)
9	Angle between λ_2, λ_{31}	μ	$\mu = \arccos\frac{\lambda_2^2+\lambda_{31}^2-\Delta^2}{2\lambda_2\cdot\lambda_{31}}$	(22)
10	External angle λ_{11}-λ_{31}	γ	$\gamma = \mu+\gamma_{05}-\gamma_{04}$	(23)
11	Angle λ_{11} to λ_{12}	α_{12}	$\alpha_{12} = \alpha_{01}+arctg\frac{\lambda_r-\lambda_{31}\cdot\sin\zeta_0}{0.5(W_0-H_0\cdot tg\zeta_0)}$	(24)
12	Internal angle λ_{31}-λ_{11}	γ_{011}	$\gamma_{011} = \pi-\gamma$	(25)
13	Angle λ_{31} to λ_{12}	γ_{06}	$\gamma_{06} = \gamma_{011}-\alpha_{12}$	(26)
14	Axis between joint B and O_2	ρ	$\rho = \sqrt{\lambda_{12}^2+\lambda_{31}^2-2\lambda_{12}\cdot\lambda_{31}\cdot\cos\gamma_{06}}$	(27)
15	Angle ρ to λ_{12}	β_{02}	$\beta_{02} = \arccos\frac{\lambda_{12}^2+\rho^2-\lambda_{31}^2}{2\lambda_{12}\cdot\rho}$	(28)
16	Angle ρ to λ_{41}	β_{03}	$\beta_{03} = \arccos\frac{\lambda_{41}^2+\rho^2-\lambda_{32}^2}{2\lambda_{41}\cdot\rho}$	(29)
17	Angle λ_{41} to λ_{12}	β	$\beta = \beta_{03}-\beta_{02}$	(30)
18	Projection of λ_{41}	y_{11}	$y_{11} = \lambda_{41}\cdot\sin(\alpha_{01}+\beta)$	(31)
19	Relative displacement	S_i	$S_i = 2y_{11}-5.8$	(32)

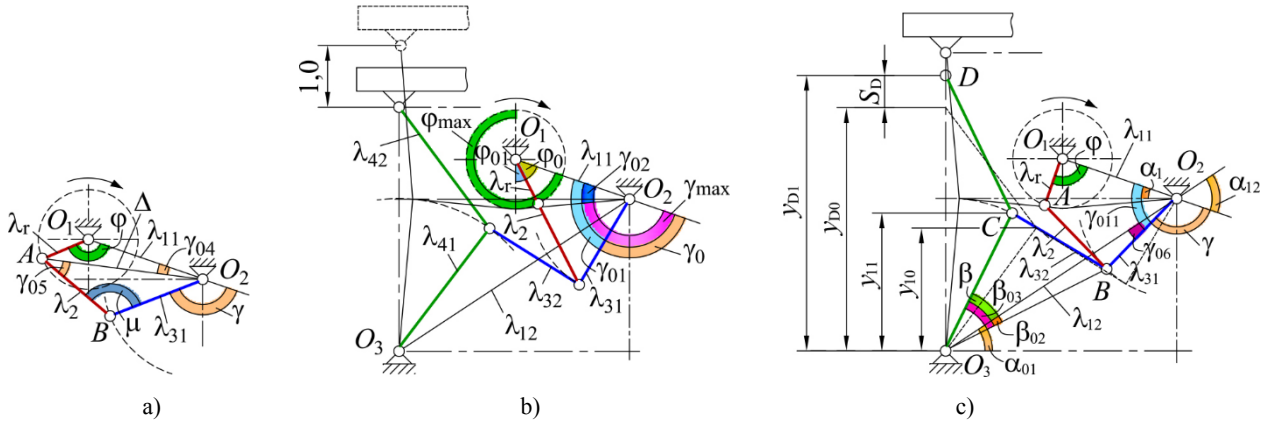

Figure 3. Schemes of the double-wedging drive mechanism for the pressure plate (left contour) in the die-cutting press for: a) justification of the phase angles of the crank and the right lever of the horizontal wedging mechanism; b) current angles of the crank, connecting rod, and right lever of the horizontal wedging mechanism; c) determination of the relative current displacement of the pressure plate

2.4 Force Load Evaluation

The following input parameters are adopted for the force load analysis of the pressure plate drive.

Force parameter:

F_t= 0.5 (Fig. 4a) - relative technological resistance to die-cutting the cardboard blank. This includes the deformation of the ejection pads on the die, cutting along the contours, and creasing the fold lines by the pressure plate actuated by the wedging mechanisms of the left contour.

Linear geometric parameter:

Δ_T - relative initial geometric sum of the cardboard thickness and the height of the ejection pads above the cutting rule edges. When die-cutting is completed, this linear parameter reaches a value of "0."

The analytical expressions required for evaluating the force loading of the wedging drive mechanism on the left contour are summarized in Table 3.

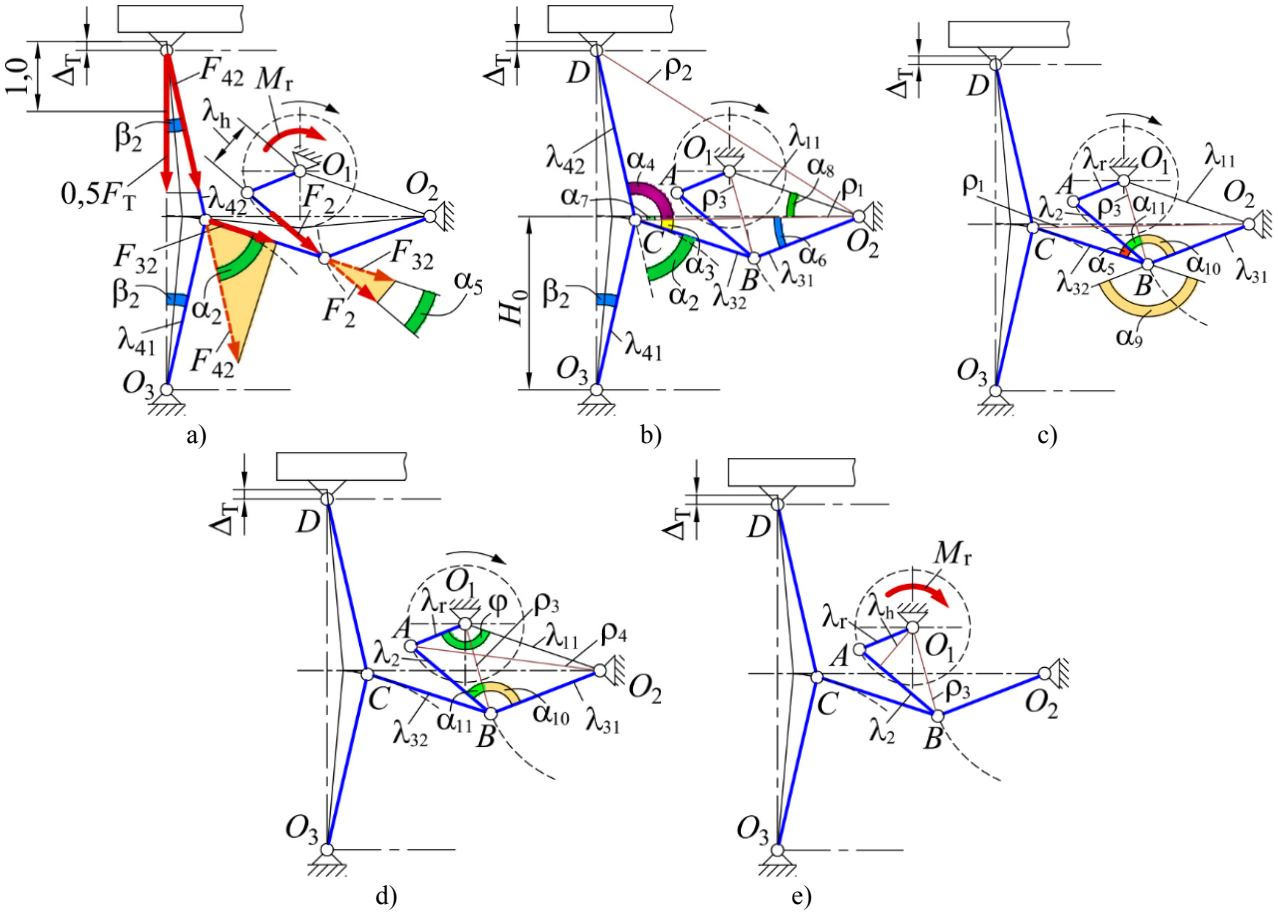

Figure 4. Schemes of the double-wedging drive mechanism for the pressure plate (left contour) in the die-cutting press for force parameter evaluation: a) determination of the angles between the levers of the vertical wedging mechanism and the vertical axis; b) construction of the force interaction geometry in the vertical contour; c) determination of angles and distances in the horizontal contour for force assessment; d) justification of the moment arm calculation in the crank-slider mechanism; e) determination of the force moment acting on the crank during the die-cutting process.

Table 3. Analytical Expressions for Force Load Evaluation

No.	Parameter Description	Notation	Analytical Expression	Eq.
1	Angle between λ_{41} (λ_{42}) and vertical (Fig.4 a)	β_2	$\beta_2 = \arccos\frac{H_0 - 0.5\Delta_t}{\lambda_{42}}$	(33)
2	Relative force along λ_{42}	F_{42}	$F_{42} = \frac{0.5}{\cos\beta_2}$	(34)
3	Axis between joints O_2 and C (Fig. 4 b)	ρ_1	$\rho_1 = \sqrt{\left(H_0 - \lambda_{41}\cdot\cos\beta_2\right)^2 + \left(W_0 - \lambda_{41}\cdot\sin\beta_2\right)^2}$	(34)
4	Angle between axis ρ_1 and link λ_{32}	α_3	$\alpha_3 = \arccos\frac{\rho_1}{2\cdot\lambda_{32}}$	(35)
5	Angle between link λ_{42} and axis ρ_1	α_4	$\alpha_4 = \arccos\frac{\lambda_{42}^2 + \rho_1^2 - \rho_2^2}{2\cdot\lambda_{42}\cdot\rho_1}$	(36)
6	Angle between λ_{32} and λ_{42} extension	α_2	$\alpha_2 = \pi - \alpha_3 - \alpha_4$	(37)
7	Relative force along λ_{32}	F_{32}	$F_{32} = F_{42}\cdot\cos\alpha_2$	(38)
8	Angle between λ_{31} and axis ρ_1	α_6	$\alpha_6 = \arccos\frac{\rho_1}{2\cdot\lambda_{31}}$	(39)
9	Angle between ρ_1 and horizontal	α_7	$\alpha_7 = \arccos\frac{W_0 - \lambda_{41}\cdot\sin\beta_2}{\rho_1}$	(40)
10	Angle between λ_{11} and horizontal	α_8	$\alpha_8 = \arccos\frac{0.5\left(W_0 - H_0\cdot tg\zeta_0\right)}{\lambda_{11}}$	(41)
11	Axis between joints O_1 and B	ρ_3	$\rho_3 = \sqrt{\lambda_{31}^2 + \lambda_{11}^2 - 2\lambda_{31}\cdot\lambda_{11}\cdot\cos\left(\alpha_6 + \alpha_7 + \alpha_8\right)}$	(42)
12	Angle between λ_{31} and λ_{32} (Fig. 4 c)	α_9	$\alpha_9 = \arccos\frac{\lambda_{32}^2 + \lambda_{31}^2 - \rho_1^2}{2\cdot\lambda_{32}\cdot\lambda_{31}}$	(43)
13	Angle between λ_{31} and axis ρ_3	α_{10}	$\alpha_{10} = \arccos\frac{\rho_3^2 + \lambda_{31}^2 - \lambda_{11}^2}{2\cdot\rho_2\cdot\lambda_{31}}$	(44)
14	Angle between λ_2 and axis ρ_3	α_{11}	$\alpha_{11} = \arccos\frac{\lambda_2^2 + \rho_3^2 - \lambda_r^2}{2\cdot\lambda\cdot\rho_1}$	(45)
15	Angle between λ_{32} and λ_2	α_5	$\alpha_5 = \alpha_9 - \left(\alpha_{10} + \alpha_{11}\right)$	(48)
16	Relative force along λ_2	F_2	$F_2 = F_{32}\cdot\cos\alpha_5$	(49)
17	Axis between joints O_2 and A (Fig. 4 d)	ρ_4	$\rho_4 = \sqrt{\lambda_2^2 + \lambda_{31}^2 - 2\lambda_2\cdot\lambda_{31}\cdot\cos\left(\alpha_{10} + \alpha_{11}\right)}$	(50)
18	Crank angle	φ	$\varphi = \arccos\frac{\lambda_r^2 + \lambda_{11}^2 - \rho_4^2}{2\lambda_r\cdot\lambda_{11}}$	(51)
19	Lever arm for F_2 (Fig. 4 e)	λ_h	$\lambda_h = \sqrt{\lambda_r^2 - \left(\frac{\lambda_r^2 - \rho_3^2 + \lambda_2^2}{2\lambda_2}\right)^2}$	(52)
20	Relative moment to overcome the die force	M_r	$M_r = F_2\cdot\sqrt{\lambda_r^2 - \left(\frac{\lambda_r^2 - \rho_3^2 + \lambda_2^2}{2\lambda_2}\right)^2}$	(53)

3. CAD/CAE ANALYSIS

Recent research highlights the effectiveness of integrating Python, ROS, and MoveIt for adaptive tool control and modeling similar tasks, such as robotic welding, as presented in research [28]. That study featured SolidWorks modeling and developing a parameterized programmatic interface for automated trajectory execution based on input geometric parameters. This interdisciplinary approach confirms the value of virtual models in the preliminary evaluation of design solutions. Similar methods of kinematic and dynamic analysis using SolidWorks Motion are also described in the study [29].

3.1 Modeling and Virtual Simulation in SolidWorks

For the preliminary analysis of the pressure plate drive, a 3D model of the proposed double-wedging mechanism was created in SolidWorks (Fig. 5). It is important to emphasize that this model is a research prototype

intended to analyze the mechanism's kinematics and motion behavior. It provides the full set of features ne–cessary for manufacturing a physical prototype (such as fastener elements, clearances, tolerances, real materials, and joint types).

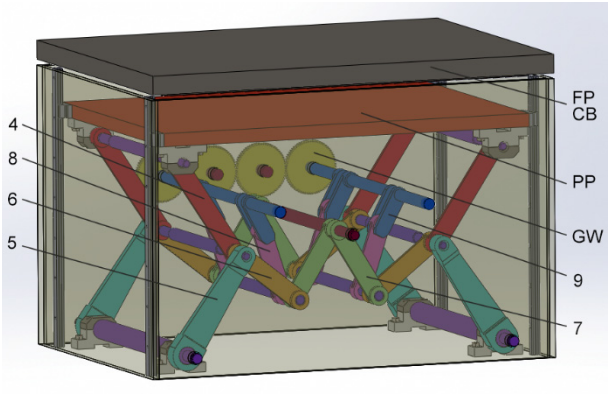

Figure 5. 3D model of the studied double-wedging mecha–nism in SolidWorks

The model was developed based on the kinematic diagram (Fig. 1) and includes the following simulated components:

-FP - die-cutting tool mounted on the fixed upper plate;

-PP - pressure plate (movable);

-CB - cardboard;

-GW - gear transmission system (gears 11, 10_1, 10_2, 12);

-Levers of the vertical and horizontal wedging mec–hanisms 4, 5, 6, 7 (4_1, 5_1, 6_1, 7_1, 4_2, 5_2, 6_2, 7_2);

-Connecting rods 8 (8_1, 8_2) and cranks 9 (9_1, 9_2);

Shaft supports (O_1, O_2), housing elements, and guides.

3.2 Python-Based Automation and Integration with SolidWorks

To automate the analysis, a Python-based software tool was developed using the COM interface to interact with SolidWorks. This tool performs analytical calculations of geometric parameters based on the formulas derived during the research and automatically launches the simulation of the model in the Motion Study envi–ronment. Python-based environments are also actively used to configure and run kinematic simulation models for verification and monitoring workflows (digital-twin style), as shown in [30].

Main Functions of the Software:

-Calculates mechanism parameters (link lengths, angles, and overall dimensions) based on the specified press pair dimensions;

-Generates a text file (equations.txt) with the calcu–lation results, which can be used as input parameters for the CAD model;

-Automatically opens a specified assembly model in SolidWorks and launches a Motion Study via the COM interface;

-Opens graphs of primary characteristics (displace–ment, velocity, acceleration, torque) after simulation completion.

This integration of the analytical model with the 3D modeling environment enabled the creation of a flexible tool for studying the behavior of the pressure plate drive across various press-pair configurations. These formats are used in the BOBST series of flatbed die-cutting presses, including models SP 76, SP 102, SP 103, SP 130, SP 142, and SP 162.

For example, the SP 162 CER model [31] is de–signed for high-performance die-cutting of cardboard blanks in the 1620×1120 mm format and is widely used in packaging for food, beverages, electronics, and hou–sehold chemicals.

This approach significantly enhances the accuracy and efficiency of preliminary design evaluations and re–duces the time required for engineering solution vali–dation. Related kinematic pipelines combining direct/inverse kinematics with Python-supported virtual models for program verification have also been demon–strated in [32] for multi-axis mechanism/machine kine–matic modeling.

The expressions in the program compute the lengths of levers, diagonals, link dimensions, gear sizes, etc. The mechanism model is parameterized to enable auto–mated adaptation to various cardboard blank formats. Each component (levers, connecting rods, pressure plate, etc.) includes key geometric parameters tied to global variables. The values of these variables are read from an external equations.txt file generated by the software, based on the selected machine size. This app–roach allows rapid 3D model updates without manually editing sketches or geometry, which is particularly beneficial when developing a format series for die-cutting presses.

SolidWorks Motion was used to perform kinematic modeling of the cycle using the assembled model. The drive is implemented via rotation of the driving gear (11, Fig. 1), which synchronously rotates the cranks of both the left and right contours. The mechanism trans–mits rotational motion via crank-slider systems to the wedging levers, thereby enabling the pressure plate to translate.

4. RESULTS

Based on the results of geometric synthesis, the relative geometric parameters of the double-wedging drive mec–hanism of the pressure plate were determined. These are: λ_r = 0.963 - the length of the driving crank; λ_{11} = 2.47 - the inter-base distance between axes O_1 and O_2; λ_{12} = 6.046 - the inter-base distance between axes O_2 and O_3; λ_2 = 1.926 - the length of the connecting rod in the driving contour; $\lambda_{31} = \lambda_{32}$ = 2.36 - the lengths of the lever and the connecting rod of the horizontal wedging mechanism; $\lambda_{41} = \lambda_{42}$ = 3.413 - the lengths of the lower and upper levers of the vertical wedging mechanism. The relative maximum displacement of the plate was assumed to be S = 1. The relative base dimensions matched the wedging mechanism used in the Bobst die-cutting press. The analysis of displacement S_i, velocity V_i, and acceleration W_i of the double-wedging mecha–nism was conducted using the derived analytical expre–ssions in relative units concerning the rotation angle φ (in degrees) of the driving crank. The corresponding calculation results are shown in Fig. 6. Here, φ_{11}, φ_{21}, and φ_{31} represent the starting angles, while φ_{12}, φ_{22}, and

φ_{32} denote the ending angles of contact between the pressure plate and the cardboard blank with respective thicknesses of Δ_{CB} = 0.3, 0.6, and 1.0 mm. The crank rotation angle during which contact with the pressure plate occurs for cardboard thickness Δ_{CB} = 0.3 mm is $\Delta_{\varphi 1} = \varphi_{32} - \varphi_{31}$; for Δ_{CB} = 0.6 mm it is $\Delta_{\varphi 2} = \varphi_{22} - \varphi_{21}$; and for Δ_{CB} = 1.0 mm it is $\Delta_{\varphi 3} = \varphi_{12} - \varphi_{11}$.

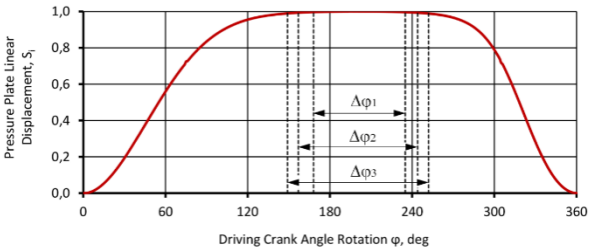

Figure 6. Graphical dependencies of the relative kinematic parameters of the double-wedging drive mechanism of the pressure plate

During the mechanism simulation in SolidWorks, the kinematic parameters were analyzed in absolute terms with respect to time t (in seconds), then converted to dependencies on the crank angle $\varphi = \pi n/30 \cdot t$. The absolute displacement of the pressure plate was set to S_{max} = 100 mm, corresponding to large-format die-cutting presses (1020×720 mm and above) produced by Bobst. The crank rotation speed was n = 60 rpm, making the duration of one full plate movement cycle T = 1 second. To objectively evaluate the obtained analytical dependencies and compare them with the SolidWorks simulation results, an analysis of the mechanism's kinematic parameters in absolute values was performed using the following expressions [23]:

$$S = S_i \cdot [S_{\max}] \tag{54}$$

$$V = V_i \cdot [S_{\max} \cdot \omega_r] \tag{55}$$

$$w = w_i \cdot \left[S_{\max} \cdot \omega_r^2 \right] \tag{56}$$

where ω_r = n/30 - angular velocity of the driving crank.

The results of calculating the absolute values of the kinematic parameters of the combined dual-wedging drive mechanism for the pressure plate are presented in Figs. 7-9. Figures 7a, 8a, and 9a show the graphical results obtained through analytical calculations, while Figs. 7b, 8b, and 9b illustrate the results obtained from the kinematic simulation of the mechanism using SolidWorks.

A comparative analysis of the graphical dependencies obtained analytically and through

SolidWorks simulation demonstrates close agreement in both the trend and the quantitative values. For the displacement function $S = f(\varphi)$, both the analytical results (Fig. 7a) and the SolidWorks simulation (Fig. 7b) show complete overlap. As seen in these dependencies, there is a steep increase in displacement in the range φ = 0°-120°, followed by a deceleration phase from φ = 120° to 150°. Beyond this range, the displacement increases only slightly (by up to 1 mm), reaching a maximum of S_{max} = 100 mm at φ = 202°. The displacement during the return motion of the plate is notably more abrupt, indicating a shorter idle stroke.

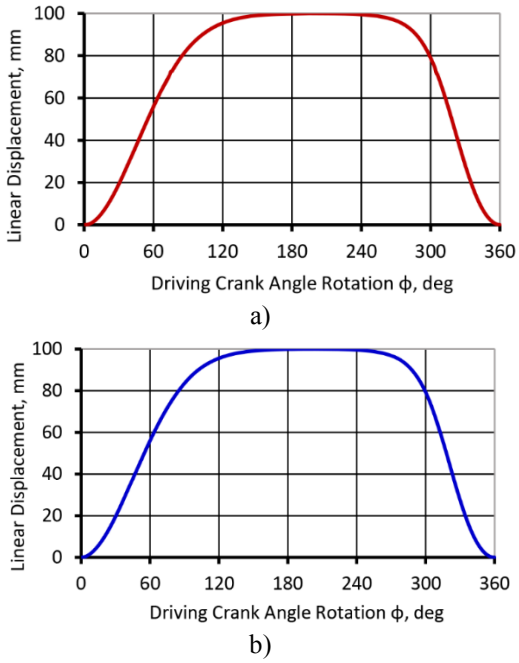

Figure 7. Linear displacement of the pressure plate obtained analytically (a) and via SolidWnorks simulation (b)

The study revealed that, for the dual-wedging mechanism, the crank rotation angles corresponding to the beginning and end of contact between the pressure plate and the cardboard blank are (Fig. 6):

-for a cardboard thickness of Δ_{CB} = 1.0 mm: $\Delta_{\varphi 1} = \varphi_{32} - \varphi_{31}$ = 252° - 149° = 103°;

-for a thickness of Δ_{CB} = 0.6 mm: $\Delta_{\varphi 2} = \varphi_{22} - \varphi_{21}$ = 244° - 157° = 87°;

-for a thickness of Δ_{CB} = 0.3 mm: $\Delta_{\varphi} = \varphi_{12} - \varphi_{11}$ = 235° - 168° = 67°.

The extended contact between the pressure plate, the cardboard blank (CB), and the embossing or creasing form ensures high-quality performance in operations that require prolonged deformation under pressure. For comparison, in Bobst presses equipped with a conventional wedging mechanism, the 1 mm thick cardboard contact angle is Δ_{φ} = 48°. The proposed dual-wedging mechanism provides a 2.15-fold increase in contact duration compared to the conventional design.

An important feature of the proposed mechanism is the asymmetry in the durations of the working (ascending) and idle (descending) strokes of the pressure plate during contact with the CB. For instance, with Δ_{CB} = 1 mm, the crank rotation angle during the upward movement is φ_h = 202° - 149° = 53°, while during the downward movement it is φ_d = 252° - 202° = 50°. This enables a sufficiently long compression phase of the cardboard, promoting the formation of the required residual deformation during creasing or embossing. The difference in durations of the working and idle strokes is a consequence of the combined design of the pressure plate drive mechanism.

The analysis of the pressure plate velocities (Fig. 8) reveals a deviation of approximately 1.9% between the negative peak velocity values, with V = -0.683 m/s obtained from analytical calculations and V = -0.696 m/s from the SolidWorks simulation. For the maximum negative peak acceleration values (Fig. 9), the discre–

pancy between the analytical results and the SolidWorks simulation is 4.6%, with w = -6.917 m/s² and w = -6.599 m/s², respectively. These results confirm the validity of the derived analytical expressions used to calculate the parameters of the combined dual-wedging drive mecha–nism of the pressure plate.

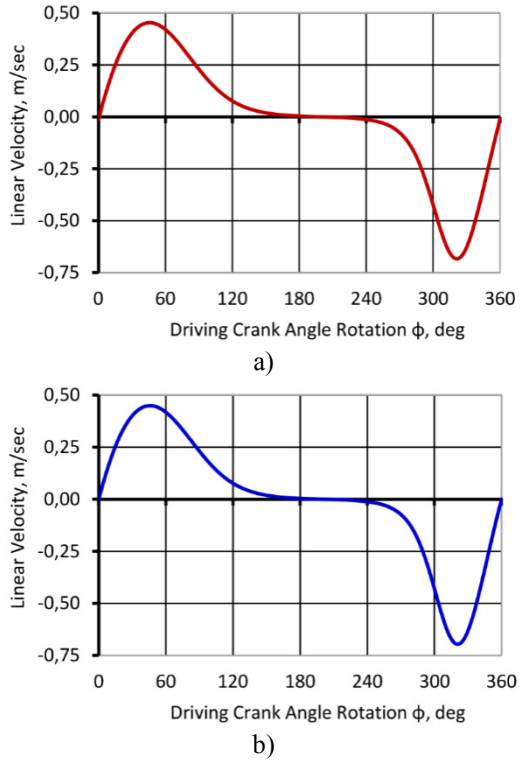

Figure 8. Linear velocity of the pressure plate obtained analytically (a) and via SolidWorks simulation (b)

It is noteworthy that during the technological ope–ration, the linear velocity of the pressure plate remains minimal. For instance, for cardboard with a thickness of Δ_{CB} = 1 mm, the velocity changes from 0.020 m/s at the moment of initial contact with the cardboard to -0.024 m/s at the end of contact. At an angle of φ = 202°, the plate's velocity reaches V = 0.00 m/s and then reverses direction.

The acceleration of the plate during its contact with the cardboard is also minimal, ranging from w = -0.35 m/s² to w = -0.52 m/s² for Δ_{CB} = 1 mm.

Figure 10 shows the torque curves obtained analy–tically (curve 1) and via SolidWorks simulation (curve 2), representing the overcoming of technological resis–tance during the crankshaft rotation. The graphs are plotted for cardboard with a thickness of Δ_{CB} = 1 mm. As shown in Fig. 10, the torque curves exhibit similar trends. The difference in the peak torque values amo–unts to Δ_{Mmax} = 147 N·m, or 5.3%, with M_{max2} = 2747 N·m in the SolidWorks simulation and M_{max1} = 2600 N·m from the analytical model. Whether SolidWorks accounts for factors such as elastic properties, clearances, friction, or inertia forces may explain this 5.3% difference.

The rapid increase in torque during the initial phase (at φ_{31} = 149°) is attributed to the onset of contact bet–ween the pressure plate and the cardboard, which generates die-cutting forces. At this point, the cutting rules induce compressive stresses that initiate a fracture front in the cardboard. This results in a subsequent drop in resistance and, consequently, a reduction in torque on the drive shaft. Simultaneously, during the upward motion of the pressure plate, the moment arm λ_h of the technological force 0.5FT decreases, reaching λ_h = 0 at the plate's topmost position (φ = 202°), at which point the resisting torque becomes M_r = 0.

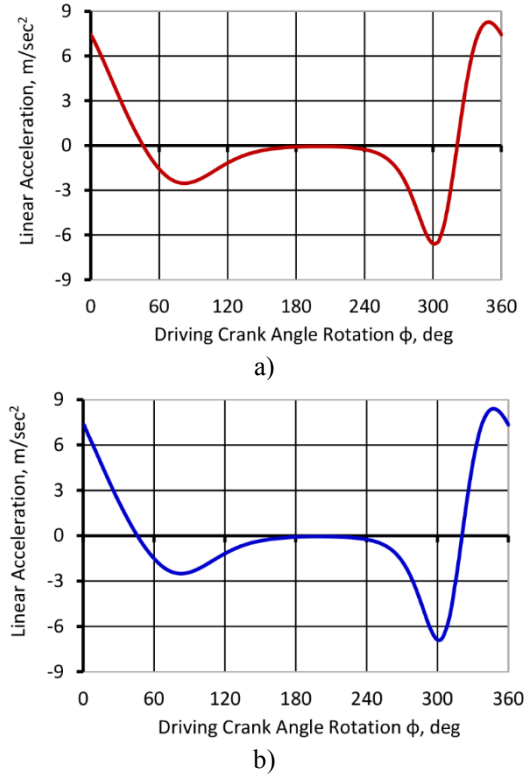

Figure 9. Linear acceleration of the pressure plate obtained analytically (a) and via SolidWorks simulation (b)

The earlier rise of the torque curve (2) by approximately 3° relative to the analytical curve (1) in the crankshaft rotation cycle (Fig. 10) may be due to specific features of the SolidWorks simulation.

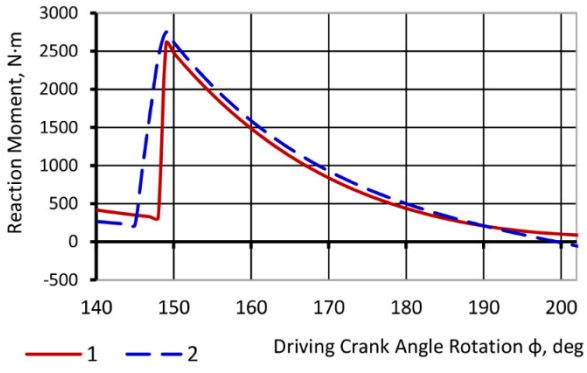

Figure 10. Torque versus crankshaft angle obtained analytically (1) and via SolidWorks simulation (2)

The moment diagrams in SolidWorks differ from analytical ones because SolidWorks employs numerical simulation, which accounts for geometry, boundary conditions, and the distribution of deformations within the body, even in the absence of applied forces or assigned material properties. In contrast, analytical calculations are based on mathematical models and

idealized loading conditions, resulting in precise but simplified outcomes.

5. CONCLUSION

A review of scientific studies in the field of die-cutting press improvement has shown that most research efforts focus on the physical and mechanical properties of cardboard, the geometry of embossing tools, and the application of advanced technologies (e.g., ultrasound) to enhance the accuracy of relief formation. A notable limitation of the existing research is its reliance on traditional wedging mechanisms, which provide only limited contact between the pressure plate and the cardboard. Additionally, the oscillatory motion of the pressure plate poses challenges during equipment setup and often fails to deliver the required die-cutting precision.

A new configuration of a dual-wedging drive mechanism has been proposed to extend the contact duration between the pressure plate and the cardboard blank. This mechanism comprises left and right contours, each including a drive system and horizontal and vertical wedging mechanisms. Such a design ensures parallel motion of the pressure plate relative to the die-cutting form throughout the entire cycle. A geometric synthesis of the mechanism was performed, yielding its relative geometric parameters. The synthesis was based on the fundamental dimensions of an existing wedging mechanism used in Bobst die-cutting presses.

A method for calculating the relative kinematic parameters of the combined double-wedging mechanism was developed. This method's universality allows for the computation of absolute kinematic values for presses of various format sizes. The unit of measure was defined as the relative linear displacement $S = 1$ of the driven link, i.e., the pressure plate.

Mathematical models of the kinematic parameters of the double-wedging mechanism were constructed. Analysis of these models showed that the contact duration of the pressure plate with 1 mm-thick cardboard is 2.15 times longer compared to the conventional wedging mechanism.

To objectively validate the analytical results, a virtual experiment was conducted in SolidWorks using a 3D model built based on the derived analytical relationships. The simulation results for the kinematic parameters of the dual-wedging mechanism closely matched the analytical findings. The deviations, within acceptable limits, were 1.9% for peak velocity values and 4.6% for peak acceleration values of the pressure plate. These results confirm the accuracy of the developed mathematical models.

Mathematical models of the resisting torque due to technological forces were also developed. For comparison, the resisting torque was determined through a virtual experiment in SolidWorks. The discrepancy between the analytical and simulation results was 5.3%.

Thus, the implementation of a combined dual-wedging mechanism incorporating both horizontal and vertical wedging components enables more than twice the contact duration between the pressure plate and the cardboard blank. This extended contact provides favorable conditions for achieving the required residual deformation during the creasing and embossing of cardboard materials.

REFERENCES

[1] Ohirko M.O. et al., 2024, "Investigation of the influence of packaging cardboard surface topography on the quality of printed products," Optical and Quantum Electronics in Computer and Intellectual Technologies, 48(2), pp. 135-140. DOI: 10.31649/1681-7893-2024-48-2-135-140

[2] Zhang, Z. et al., 2023, "Enhancing the recyclability of packaging by design: An analysis of packaging materials in the circular economy," Resour. Conserv. Recycl., 190, pp. 106871. DOI:10.1016/j.resconrec.2022.106871

[3] Kolekar, S. C., Satao, S., 2022, "A Review of Implementation of Green Manufacturing in Die-Cutting Industry," Pratibodh Journal for Engineering, 2(1). Available at: https://pratibodh.org

[4] Jiao, L. Q., Wang, Y. M., Wu, S. Q., Li, L. H., 2018, "Study on Pressure Testing Method of Die-Cutting Machine Based on Micro-capsule and Image Sensor," Proc. ICMEIT, pp. 32-38. DOI:10.12783/dtetr/icmeit2018/23377

[5] Pevec, P., Kapun, T., Gregor-Svetec, D., 2025, "Recyclability of Intelligent Cardboard Packaging," Sustainability, 17(7), pp. 2924. DOI:10.3390/su17072924

[6] Zhang, H., Liu, Yand Li, Z., 2018, "Passive velocity field control for die-cutting machine," J. Phys.: Conf. Ser., 1074, pp. 012025. DOI: 10.1088/1742-6596/1074/1/012025

[7] Lin, W. G., Zhou, C., Huang, W. J., 2015, "Optimum Design for Mechanical Structures and Material Properties of the Dual-Elbow-Bar Mechanism," Adv. Mater. Sci. Eng., pp. Article ID 724171. DOI: 10.1155/2015/724171

[8] Zhou, Y., Cheng, B., Yang, H., Wang, C., 2024, "Simulation of the Relationship Between Die-Cutting Moving Platform and Crankshaft Motion," FAIA, 382, pp. 148-153. DOI: 10.3233/FAIA231293

[9] Wang, J., Chen, X., and Li, Y., 2023, "Structure Design and Optimization Algorithm of a Lightweight Drive Rod for Precision Die-Cutting Machine," Appl. Sci., 13, pp. 4211. DOI: 10.3390/app13074211

[10] Ivanko, A., Zenkin, M., Chernysh, M., Kolinko, I., 2024, "Improvement of the Pneumatic Drive of a Flat Die-Cutting Press," Tech. Sci. Technol., 4(38), pp. 70-79. DOI: 10.25140/2411-5363-2024-4(38)-70-79

[11] Vlakh, V. V., Mykhailiv, Yu. Yu., 2023, "Research on the pressure plate movement by the drive with wedging mechanisms in the die-cutting press," Printing and Publishing, 2(86), pp. 174-184. DOI: 10.32403/0554-4866-2023-2-86-174-184

[12] Knysh, O., Rehei, I., Kandiak, N., Ternytskyi, S., Ivaskiv, B., 2022, "Experimental Evaluation of

Eccentric Mechanism Power Loading of Movable Pressure Plate in DieCutting Press," Acta Mech. Autom., 16(3), pp. 266-273. DOI: 10.2478/ama-2022-0032

[13] Ternytskyi, S., Rehei, I., Kandiak, N., Radik–hovskyi, I., Mlynko, O., 2021, "Experimental Re–search of Paperboard Cutting in Die Cutting Press with the Screw-Nut Transmission of Drive Mec–hanism of a Movable Pressure Plate," Acta Mech. Autom., 15(3), pp. 122-131. DOI: 10.2478/ama-2021-0017

[14] Rehei, I., Ternytskyi, S., Kandiak, N., Koval, T., 2020, "Experimental Analysis of Corrugated Fibre–board Cutting with Movable Cutting Disc During Large-Sized Package Manufacture," Aust. J. Mech. Eng. DOI: 10.1080/14484846.2020.1747734

[15] Rehei, I., Vlakh, V., Mykhailiv, Y., 2023, "Technical Justification of the Sectional Const–ruction of the Pressure Plate in the Die-Cutting Press," Proc. Int. Sci. Discussion Conf..DOI: 10. 51582/interconf.19-20.03.2023.055

[16] Knysh, O., Rehei, I., Vlakh, V., Mlynko, O., Ternytskyi, S., 2023, "Analytical Interpretation of Experimental Research of Cardboard Cutting in Die-Cutting Press," Acad. J. Manuf. Eng., 21(1), pp. 43-49

[17] Rehei, I., Knysh, O., Vlakh, V., Mykhailiv, Y., 2023, "Sectional Design of the Pressure Plate in the Die-Cutting Press with Wedging Mechanisms: Justification of Application," Proc. 1st Int. Sci. Pract. Conf. Modern Knowledge. DOI: 10.51582 /interconf.19-20.05.2023.031

[18] Hünniger, J., Engisch, L., Hamblyn, S., Käppeler, U., Hofmann, A., 2022, "Influence of Ultrasound on Embossing Results for Cardboard," BioRe–sources, 17(4), pp. 5803-5819. DOI: 10.15376/ biores.17.4.5803-5819

[19] Käppeler, U., Hünniger, J., Hofmann, A., Berlich, A., Engisch, L., 2020, "Thermal Influence on the Mechanical Properties of Cardboard during an Ultrasonic-Assisted Embossing Process," Bio Re–sources, 15(3), pp. 5110-5121. DOI: 10.15376/ biores.15.3.5110-5121

[20] Käppeler, U., Schneller, K., Wallburg, F., Engisch, L., Schoenfelder, S., 2022, "Analysis of the Com–pression Behavior of Different Cardboard Materials during Embossing," Open Conf. Proc., 2, pp. 132. DOI: 10.52825/ocp.v2i.132

[21] Rehei, I., Vlakh, V., Knysh, O., Mlynko, O., 2023, "Combined Double Crank Wedging Drive Mecha–nisms of the Press Plate Used in Die-Cutting Press: Synthesis, Kinematic and Functional," Acad. J. Manuf. Eng., 21(3), pp. 53-60

[22] Vlakh, V. V., 2023, "Comparative Analysis of the Kinematic Parameters of the Wedging Drive Mechanisms of the Die-Cutting Presses Using the SolidWorks Software," Printing and Publishing, 1(85), pp. 174-183.

[23] DOI: 10.32403/0554-4866-2023-1-85-174-183

[24] Vlakh, V. V., Rehei, I. I., Knysh, O. B., 2025, "Re–search of the wedging mechanism with additional driven crank and gear transmission in the pressure plate drive of the die-cutting press," Aust. J. Mech. Eng. DOI: 10.1080/14484846.2025.2459456

[25] Liu, Y., and Ben-Tzvi, P. (March 15, 2021). "A New Extensible Continuum Manipulator Using Flexible Parallel Mechanism and Rigid Motion Transmission." ASME. J. Mechanisms Robotics. June 2021; 13(3): 031014. https://doi.org/10.1115/ 1.4050097

[26] Bai, G., Kong, X., Ritchie, J. M. (March 24, 2017). "Kinematic Analysis and Dimensional Synthesis of a Meso-Gripper." ASME. J. Mechanisms Robotics. June 2017; 9(3): 031017. https://doi.org/10.1115/ 1.4035800

[27] Shihora, N. et al (January 20, 2025). "On the Use of Tension Transition Zones for Kinematic and Compliance Performance Analysis of Wire-Actuated Continuum Robots." ASME. J. Mecha–nisms Robotics. June 2025; 17(6): 061013. https:// doi.org/10.1115/1.4067432

[28] McCarthy, J. M. (May 4, 2011). "21st Century Kinematics: Synthesis, Compliance, and Tenseg–rity." ASME. J. Mechanisms Robotics. May 2011; 3(2): 020201. https://doi.org/10.1115/1.4003181

[29] Puthussery, S., Secco, E. L., 2024, "Design and inte–gration of a robotic welding parameterized proce–dure for industrial applications," Spektrum–Industri, 22(1), pp. 6076. DOI: 10.12928/si.v22i1 .179

[30] Popkonstantinovic, B., Stojicevic, M., Jelic, Z., Obradovic, M., PopaDragos-Laurentiu, 2019, "Si–mulation and Motion Study of Mechanical Integ–rator 3D Model", FME Transactions, 47(2), pp. 299–303. doi:10.5937/fmet1902299P.

[31] Vorkapic, N., Zivanovic, S., Dimic, Z., Kokotovic, B., Slavkovic, N., 2021,"Virtual Horizontal Machi–ning Center LOLA HBG 80 for Program Verifi–cation and Monitoring", FME Transactions, 49(3), pp. 696–703. doi:10.5937/fme2103696V.

[32] BOBST, "SP 162 CER - Automatic die-cutter with blanking." Available at: https://www.bobst.com/ usen/products/flatbed-die-cutting/diecutters/over view/machine/sp-162-cer/

[33] Slavkovic, N., Dimic, Z., Zivanovic, S., Miluti–novic, M., 2018,"Kinematic Modeling of 5-axis Horizontal Milling Machine Emulated From Verti–cal Articulated Robot", FME Transactions, 46(1), pp. 46–56.doi:10.5937/fmet1801046S.

NOMENCLATURE

S	maximum relative displacement of the pressure plate
W_0	relative horizontal distance between the supports of the double-wedging mechanism on the left contour
H_0	relative vertical distance between the supports of the double-wedging mechanism on the left contour
Si	relative displacement

Vi	relative velocity
wi	relative acceleration
V	absolute velocity of the pressure plate (m/s)
w	absolute acceleration of the pressure plate (m/s²)
n	crank rotational speed (rpm)
Δ_{CB}	cardboard thickness (mm)
Δ_T	relative initial linear geometric parameter associated with the initial total cardboard thickness; decreases to 0 at the end of cutting
M_r	resisting (load) torque acting on the crank (N·m)
M_{max1}	peak torque from the analytical model (N·m)
M_{max2}	peak torque from SolidWorks simulation (N·m)
Δ_{Mmax}	difference between peak torque values (N·m)

Greek symbols

ζ_0	limiting angle for the horizontal and vertical wedging contours to prevent jamming (deg)
λ_{11}	base distance between axes O_1 and O_2
λ_{12}	base distance between axes O_2 and O_3
λ_r	crank radius
λ_2	connecting rod length
λ_{31}	lever length of the horizontal wedging mechanism
λ_{32}	connecting-rod length of the horizontal wedging mechanism
λ_{41}	lower lever length of the vertical wedging mechanism
λ_{42}	upper lever length of the vertical wedging mechanism
φ	crank angle (deg)

Acronyms

CAD	Computer-Aided Design
CAE	Computer-Aided Engineering
COM	Component Object Model
PP	Pressure Plate
FP	Fixed Plate (die-cutting tool plate)
CB	Cardboard
LC	Left Contour
RC	Right Contour
GW	Gear transmission system

ИНОВАТИВНИ МЕХАНИЗАМ СА ДВОСТРУКИМ КЛИНОМ ЗА ПРЕСЕ ЗА СЕЧЕЊЕ: КИНЕМАТИЧКА И АНАЛИЗА СИЛЕ ЗАСНОВАНА НА CAD/CAE ТЕХНОЛОГИЈИ

И. Рефеи, О. Книш, В. Влах, А. Терновиј

Овај рад представља дизајн и анализу новог погонског механизма са двоструким клином за потисну плочу пресе за сечење, предложеног као алтернатива традиционалним системима са радилицом. Механизам побољшава пренос кретања, повећава уједначеност контакта са картонском плочом и смањује инерцијална оптерећења током утискивања, пресавијања и сечења. Развијена је кинематичка шема и изведени су аналитички изрази за померање и обртни момент. Прилагођени Python алат аутоматизује израчунавање параметара, гене–рисање модела и интеграцију са SolidWorks-ом за симулацију и оптимизацију. 3D модели и студије кретања валидирају аналитички модел. Анализа силе потврђује структурну изводљивост механизма. Предложени систем обезбеђује стабилније и ефи–касније кретање потисне плоче, чиме се побољ–шавају перформансе пресе за сечење. Интеграција Python аутоматизације са CAD/CAE алатима побољ–шава инжењерски ток рада и подржава будућу индустријску имплементацију.